Scaling of Convective Heat Transfer Enhancement due to Flow Pulsation in an Axisymmetric Impinging Jet

Tim Persoons[1]
Trinity College Dublin
Dept. Mechanical and Manufacturing Engineering,
Dublin, Ireland

Kuanysh Balgazin
Trinity College Dublin
Dept. Mechanical and Manufacturing Engineering,
Dublin, Ireland

Karl Brown
Trinity College Dublin
Dept. Mechanical and Manufacturing Engineering,
Dublin, Ireland

Darina B. Murray
Trinity College Dublin
Dept. Mechanical and Manufacturing Engineering,
Dublin, Ireland

Abstract

Impinging jets are widely used to achieve a high local convective heat flux, with applications in high power density electronics and various other industrial fields. The heat transfer to steady impinging jets has been extensively researched, yet the understanding of pulsating impinging jets remains incomplete. Although some studies have shown a significant enhancement compared to steady jets, others have shown reductions in heat transfer rate, without consensus on the heat transfer mechanisms that determine this behavior. This study investigates the local convective heat transfer to a pulsating air jet from a long straight circular pipe nozzle impinging onto a smooth planar surface (nozzle-to-surface spacing $1 \leq H/D \leq 6$, Reynolds numbers $6000 \leq Re \leq 14{,}000$, pulsation frequency 9Hz $\leq f \leq$ 55Hz, Strouhal number $0.007 \leq Sr = fD/U_m \leq 0.1$). A different behavior is observed for the heat transfer enhancement in (i) the stagnation zone, (ii) the wall jet region and overall area-average. Two different modified Strouhal numbers have been identified to scale the heat transfer enhancement in both regions: (i) $Sr(H/D)$ and (ii) $SrRe^{0.5}$. The average heat transfer rate increases by up to 75-85% for $SrRe^{0.5} \cong 8$ ($Sr = 0.1$, $Re = 6000$), independent of nozzle-to-surface spacing. The stagnation heat transfer rate increases with nozzle-to-surface distance H/D. For $H/D = 1$ and low pulsation frequency ($Sr < 0.025$), a reduction in stagnation point heat transfer rate by 13% is observed, increasing to positive enhancements for $Sr(H/D) > 0.1$ up to a maximum enhancement of 48% at $Sr(H/D) = 0.6$.

Keywords: impinging jet; pulsating flow; hot spot; high density; electronics cooling; boundary layer redevelopment.

[1] Corresponding author. E-mail: tim.persoons@tcd.ie.

Manuscript submitted on June 21, 2012 to the ASME Journal of Heat Transfer, intended for the Special Issue on High Heat Flux Cooling of Electronics.
Revised version submitted on November 5, 2012. Final version submitted on December 18, 2012.

Nomenclature

c	Speed of sound in fluid, m/s	T, T_{jet}	Surface and jet temperature, °C
C_p	Specific heat capacity of fluid, J/(kgK)	t	Time, s
D	Nozzle diameter, m	U, V	Axial and radial velocity, m/s
Fr	Frössling number ($Fr = Nu/(Re^m Pr^n)$)	u', v'	Axial and radial rms velocity fluctuation, m/s
f	Flow pulsation frequency, Hz	U_m	Nozzle-averaged axial velocity, m/s
H	Nozzle-to-impingement surface spacing, m	x, r	Axial and radial coordinate, m
h	Convective heat transfer coefficient, W/(m^{2}K)		**Greek symbols**
j	Imaginary unit	β_0	Stagnation point radial velocity gradient $(\partial V/\partial r)_0$, s^{-1}
k	Thermal conductivity of fluid, W/(mK)	Δ_A, ε_A	Absolute and relative uncertainty on quantity A
L	Nozzle length, m	δ_T	Thermal boundary layer thickness, m
Nu	Local Nusselt number ($Nu = hD/k$)	ν	Kinematic viscosity of fluid, m^2/s
Pr	Prandtl number ($Pr = \rho C_p \nu/k$)	ρ	Density of fluid, kg/m^3
p	Pressure, Pa		**Subscripts**
q	Local convective heat flux, W/m^2	$_0$	Stagnation point
Re	Reynolds number ($Re = U_m D/\nu$)	$_a$	Acoustic
Sr	Strouhal number ($Sr = fD/U_m$)	$_H$	Helmholtz resonance
St	Stokes number ($St = 2\pi f(D/2)^2/\nu$)	$_m$	Spatial average

1. Introduction

A recent review by Garimella et al. [1] outlines the challenges facing the telecommunication systems and data center industry in relation to thermal management of electronics. Increased awareness about the energy consumption of these systems, the growing data traffic volume and installed computational power have made electronics cooling a very active research field. Research activities cover a wide range of cooling techniques, from high density heat transport using novel high conductivity materials and two-phase convection systems, to high and moderate density cooling using forced liquid and air convection in micro-structured heat sinks. With the evolution towards three-dimensional chip stacking, cooling techniques that can dissipate strong spatial variations in heat flux are being developed [1]. To this end, liquid impinging jets are being considered to ensure maximal heat transfer efficiency and good spatial uniformity [2,3].

Impinging continuous jets can achieve high local heat transfer rates because the jet flow establishes very thin boundary layers. Synthetic jets do not need an external pressurized fluid supply, and synthesize a train of propagating vortices by successive ejection and suction of fluid across an orifice. These jets can yield comparable heat transfer rates to steady jets [4], and multiple adjacent synthetic jets can combine high thermal performance with fluidic control [5]. The vortices in synthetic jets periodically break up the thermal boundary layer, forcing it to redevelop at the driving frequency of the jet. Similar yet weaker vortices also form naturally in steady jets. By imposing a pulsating flow component to a continuous jet, these vortices can be reinforced. However as shown in the following section, the available literature on pulsating jet heat transfer is scattered and does not provide a clear consensus on the governing mechanisms or optimal operating conditions.

1.1. Effect of Flow Pulsation on Convective Heat Transfer

For a steady impinging jet, the convective heat transfer rate depends strongly on the flow conditions in the nozzle and their effect on the flow in the stagnation region. For an incompressible laminar impinging jet, the boundary layer equations can be solved to yield a theoretical expression for the stagnation Nusselt number $Nu_0 = C(\beta_0 D/U_m)^{1/2} Re^{0.5} Pr^{0.4}$ (neglecting any temperature effects on density and viscosity), where β_0 is the radial velocity gradient at the stagnation point ($\beta_0 = (\partial V/\partial r)_0$) and $C = 0.763$ for an axisymmetric flow [6]. Shadlesky [6] derived that $\beta_0 D/U_m = 3\pi/16$ for an axisymmetric flow with uniform nozzle velocity profile, or $Nu_0 = 0.5856 Re^{0.5} Pr^{0.4}$ [6,7]. For fully developed flow in a long pipe, the radial velocity gradient is steeper and thus the stagnation heat transfer rate is higher. Experimental results for a steady impinging jet are used in Sect. 4.1 to validate the methodology of this work. More details on the heat transfer characteristics of steady jets are given there.

Liu and Sullivan [7] used low-level fluidic excitation to reinforce the heat transfer contribution of large scale vortices which form naturally in a jet shear layer. Using an acoustic speaker mounted inside a settling chamber with an axisymmetric contoured nozzle, their rms excitation amplitude $u'/U_m \cong 10^{-4}$. The relative heat transfer enhancement varied between −10% and +10% depending on excitation frequency and H/D, however the effect is restricted to $1 < r/D < 2.5$ and is not observed in the stagnation region (H/D = 0.6–2, Re = 12,300). This behavior has been confirmed for a similar geometry (H/D = 0.5–2, Re = 10,000–30,000) by O'Donovan and Murray [8].

For pulsating jets, several studies report a significant reduction in local heat transfer rates compared to the equivalent steady jet, as shown in Table 1. Heat transfer results are given as percentages of a dimensionless enhancement factor, $\delta Nu = Nu^{(\text{pulsating})}/Nu^{(\text{steady})} - 1$. Sheriff and Zumbrunnen [9] study the heat transfer to an impinging jet covering Reynolds numbers of 2500-10,000, H/D = 2–6 and Strouhal number Sr = 0.014–0.96 (f = 5–280Hz). They report a reduction in the stagnation point Nusselt number (-60% < δNu_0 < -18%) compared to steady flow, and no change in the wall jet region. Azevedo et al. [10] observed heat transfer deterioration (-20%) for Re = 4000–40,000 and frequencies up to 200Hz. Hofmann et al. [11] report a strong reduction (-50%) near the stagnation point of a circular impinging jet for Re = 14,000–78,000. Although flow pulsation is seen to increase entrainment and the turbulence intensity in the jet core, the authors attribute the heat transfer deterioration to the overall jet velocity reduction and increased jet spread, especially at H/D > 5. Only in final experiments at Sr = 0.2 (at frequencies up to 400Hz) did they observe positive enhancements up to 40% at H/D = 2.

By contrast, other studies report significant heat transfer enhancements when pulsation is applied. For a self-oscillating two-dimensional jet, Camci and Herr [12] found enhancement factors up to 70% for Re = 14,000 and H/D = 24. Using an intermittent impinging jet generated by a rotating blade, Zumbrunnen and Aziz [13] found enhancements up to 100% at high frequency. They also formulated a hypothesis to explain the threshold for enhancement based on laminar flow theory, which agrees very well with their experiments. At stagnation, the thermal boundary layer thickness $\delta_T(\tau)$ grows to 99% of the final thickness $\delta_T(\infty)$ after a dimensionless time $\beta_0/f \cong$ 4–6 (for $0.7 < Pr < 15$), where β_0 represents the radial velocity gradient at the stagnation point. They hypothesized that the enhancement due to forced boundary layer redevelopment becomes significant when $\beta_0/f < 3$, or a minimum excitation frequency $Sr = fD/U_m > 1/3(\beta_0 D/U_m) \cong 0.262$ for a two-dimensional jet or $Sr > 0.194$ for a circular jet [6]. This analysis only applies to jets with high excitation levels, not the small levels used by Liu and Sullivan [7]. Zumbrunnen and Aziz [13] present enhancement factors as a function of the dimensionless time $\beta_0/f = (\beta_0 D/U_m)/Sr$. An enhancement of 100% is observed for $\beta_0/f < 2$, while a deterioration in performance is noted for $\beta_0/f > 6$.

A criterion based on the Strouhal number is partially confirmed by other sources. Herwig and Middelberg [14] observed an increasingly positive enhancement for $Sr > 0.029$ for a circular jet from a long pipe nozzle, up to δNu_0 = 30% at Sr = 0.076 for square-wave excitation. All studies mentioned in this review use duty cycles of 50%. While most only consider square wave excitation, Herwig and Middelberg [14] also investigated different waveform shapes, which showed that triangular and sinusoidal pulsations exhibit a much lower enhancement than a square waveform. Mladin and Zumbrunnen [15] found a stagnation point enhancement up to 12% and up to 80% in the wall jet, and conclude that high frequency fluctuations perform better than low frequency fluctuations. Similarly, Behera et al. [16] found δNu_0 = 12% in the stagnation zone, and δNu = 35% in the wall jet region, for Re = 5130 and H/D = 7 and frequencies from 25Hz to 400Hz ($0.008 < Sr < 0.13$).

Using flow visualization to compare steady and pulsating jets, Farrington and Clauncht [17] showed that the vortices in pulsating flow are stronger and form closer to the orifice. The irregular vortex pattern of steady jets is transformed by the pulsations to a more organized vortex train. These larger vortices also lead to a wider spread angle for the potential core and accelerated entrainment. Fluctuation intensities along the centerline of a pulsating jet flow are higher than for steady jets up to 3−5 diameters from the nozzle exit, but lower at distances beyond 10 diameters. This higher rate of decay is accompanied by a strong increase in turbulence intensity as kinetic energy of coherent vortices cascades into turbulent motion [17].

Similar characteristics (i.e., increased spreading, entrainment, jet decay and turbulence intensity) are observed in synthetic jets, which are zero-net mass flux jets induced by oscillating fluid motion across an orifice [18]. For the same reasons, impinging synthetic jets have excellent potential for convective heat transfer [4,5,19]. For an axisymmetric impinging synthetic jet, Persoons et al. [4] have identified different flow and heat transfer regimes based on the ratio of stroke length to nozzle-to-surface spacing. In the limit case for high stroke length, the flow field is similar to that of a pulsating jet.

Although not directly applicable to jet flows, Persoons et al. [20] show a heat transfer enhancement up to 40% by applying an inline sinusoidal pulsation to a liquid flow micro-channel heat sink. Here too, high excitation levels ($u'/U_m > 0.2$) are needed to achieve a positive enhancement although the effect of frequency is found to be negligible in the investigated range $100 < Re < 650$, $0.002 < Sr < 0.1$, $0.002 < u'/U_m < 3$, where U_m represents the mean channel velocity.

The literature review (summarized by Table 1) shows a lack of consistency, although this can be partly attributed to the wide range of jet configurations (e.g., submerged and free surface jets, axisymmetric or planar geometries, fully developed or uniform nozzle velocity profiles). There are no clear trends for the magnitude, sign and dependencies of the heat transfer enhancement due to flow pulsation. Some studies report reductions in heat transfer rates (as low as −60%) either in the stagnation zone or across the entire surface, especially at higher nozzle-to-surface spacing [9–11]. Some studies report significant enhancements (up to +100%) both near the stagnation point and in the wall jet region [12–16]. Of the aforementioned studies, only Herwig and Middelberg [14] use the same configuration as the present study (i.e., a submerged pulsating air jet issuing from a long pipe nozzle). Like for synthetic jets, the introduction of flow unsteadiness can be beneficial for heat transfer, yet a better understanding of the governing mechanisms is needed. As such, this study aims to validate some of the findings for an axisymmetric impinging pulsating air jet (for square wave excitation with a 50% duty cycle), and provide a better insight into the nature of convective heat transfer to forced unsteady jet flows.

2. Experimental Approach

Figure 1 shows a schematic diagram of the test facility. The air jet issues from a pipe nozzle (a) consisting of a smooth brass pipe with inner diameter D = 13mm and length $L = 32D$, with a sharp edged exit, chamfered externally at 45°. The pipe length exceeds the hydraulic development length for turbulent flow by about 50% for the range of Reynolds numbers under investigation ($6000 \le Re \le 14{,}000$). The pipe nozzle is connected to one outlet port of a three-way pneumatic valve (c). A second dummy pipe nozzle of identical dimensions (b) is connected to the second outlet port and mounted at the same axial distance to a secondary impingement surface (not shown in Fig. 1), which ensures identical boundary conditions when switching the flow from one branch to the other. The pneumatic solenoid operated 3-way valve (Parker Series 9, model 009-0143-900) has a response time of less than 5 milliseconds as specified by the manufacturer. The valve is driven by a power amplifier and a square wave generator with a 50% duty cycle (d). The air flow to the inlet port of the valve is supplied from the building air compressor and dehumidification system, via a pressure regulator (f), a 100 liter buffer vessel (not shown in Fig. 1), and a mass flow controller (e) (MKS 1579A, 0-300 standard liter/min) with an uncertainty of ±3 standard liter/min (including nonlinearity, hysteresis and repeatability). The uncertainty in the Reynolds number is determined via the rule of propagation of uncertainties as $\varepsilon_{Re} = \Delta_{Re}/Re \cong [(\Delta_M/M)^2 + (\Delta_D/D)^2]^{1/2}$ where Δ_M represents the uncertainty in the mass flow rate and $\Delta_D \cong 0.25$mm is the uncertainty in the nozzle diameter. The resulting uncertainty $\varepsilon_{Re} \cong 3$-6% for the investigated range, based on a 95% confidence level. For steady flow, the turbulence intensity at the nozzle exit does not exceed 8.5% of the mean velocity [21].

The distance between nozzle exit and impingement surface H is continuously adjustable. The impingement angle is fixed at 90°. The instrumented surface consists of a flat copper plate (425 x 550 mm^2, 5 mm thick). Electrical power is supplied from a DC voltage source to a 1.1 mm thick silicone rubber mat with embedded wire heaters, glued to the underside of the copper plate. The plate assembly is insulated underneath the heater mat. For typical jet Reynolds numbers, the representative Biot number $h \cdot t/k_{Cu} \cong 0.0013$ (where t = 5mm is the plate thickness). The plate approximates a constant wall temperature boundary condition which is both uniform in space and time-invariant, as verified in earlier studies [21]. The system is operated at a fixed surface temperature of 60 °C and an ambient temperature of about 25 °C.

The local convective heat transfer coefficient is defined as h (= $Nu\, k/D$) = $q/(T - T_{ref})$ where q is the local convective heat flux and T is the local surface temperature. Since the flow velocity remains well below the speed of sound in these tests ($Ma < 0.05$), the reference temperature T_{ref} is taken as the jet temperature recorded with a T-type thermocouple mounted in the air supply line upstream of the pipe nozzle. The uncertainty in the reference and surface temperature $\Delta_T < 0.1$K, based on a 95% confidence level.

The local convective heat flux q is measured with a factory calibrated RdF Micro-Foil™ differential thermopile heat flux sensor, which measures the temperature difference across a well-defined thermal barrier. The manufacturer's calibration coefficient for the heat flux sensor (0.093μV/(W/m^2)) is within 3% of the value obtained from a calibration experiment for the stagnation point Nusselt number in an impinging steady jet issuing from a contoured circular nozzle [6]. The response time of the heat flux sensor is about 0.02s [21]. For the experimental conditions encountered in this study, the radiation heat loss from the sensor accounts for about 3-6% of the convection heat flux near the stagnation point, up to a maximum of about 15% at $r/D \cong 4$. For the stagnation point, this effect is intrinsically contained in the heat flux sensor calibration, which is performed at the same surface and ambient temperature. The resulting uncertainty in the Nusselt number $\varepsilon_{Nu} = \Delta_{Nu}/Nu \cong [(\Delta_q/q)^2 + 2(\Delta_T/(T - T_{ref}))^2]^{1/2}$ equals about 6% based on a 95% confidence level, with a spatial resolution of about 1 mm in the radial direction [21].

3. Theoretical Analysis of the Pulsating Flow Velocity Profile

For a transient fully developed laminar flow in an axisymmetric pipe with negligible density changes ($\partial\rho/\rho \ll \partial U/U$) [22], the Navier-Stokes equations simplify to

$$\rho \frac{\partial U}{\partial t} = -\frac{\partial p}{\partial x} + \rho \nu \left(\frac{\partial^2 U}{\partial r^2} + \frac{1}{r}\frac{\partial U}{\partial r} \right) \tag{1}$$

where $U(r,t)$ is the axial velocity, $\partial p/\partial x(t)$ is the axial pressure gradient, ρ and ν are the density and kinematic viscosity of the fluid. For a sinusoidal pressure gradient $\partial p/\partial x = -|\partial p/\partial x|\exp(j2\pi ft)$, Eq. (1) can be solved analytically as shown by White [22] (pp. 135-136):

$$U(r,t) = \frac{1}{\rho}\left|\frac{\partial p}{\partial x}\right| \frac{e^{j2\pi ft}}{j2\pi f}\left[1 - \frac{J_0\left(\sqrt{-j\,2\pi fr^2/\nu}\right)}{J_0\left(\sqrt{-j\,2\pi f\left(\frac{1}{2}D\right)^2/\nu}\right)}\right] \tag{2}$$

where j is the imaginary unit ($j = (-1)^{1/2}$), J_0 is the Bessel function of the first kind and zeroth order, and $2\pi f(D/2)^2/\nu$ is a dimensionless frequency referred to as the Stokes number St. The shape of the oscillating flow velocity profile is characterized by St. For small Stokes numbers ($St < 100$) the flow is quasi-steady and the velocity profile is almost parabolic, similar to steady laminar flow. For $St >> 1000$ the velocity profile becomes increasingly flat. In this study, the Stokes number varies between 160 and 980 which suggest a near parabolic profile.

Although the pressure excitation due to the valve switching flow between both branches is too complicated to allow an analytical solution, it can be approximated by numerical integration of Eq. (1) in space (r) and time (t). The natural Helmholtz resonance frequency of a semi-open tube of length L equals $f_H = \sqrt{3}(c/L)/(2\pi) \cong 312$ Hz, where c is the speed of sound of air [23]. At low frequency ($f < \frac{1}{2}f_H$), the effect of compressibility in the pipe nozzle can be lumped into an acoustic impedance consisting of a series combination of acoustic mass and compliance $p_a/U_m = \rho Ls\cdot[(jf/f_H)^2 + 1]^{-1}$. Incorporating this acoustic pressure fluctuation in Eq. (1) yields:

$$\left(\rho\frac{f^2}{f_H^2 - f^2}\right)\frac{\partial U}{\partial t} = -\frac{\partial p}{\partial x} + \rho\nu\left(\frac{\partial^2 U}{\partial r^2} + \frac{1}{r}\frac{\partial U}{\partial r}\right) \tag{3}$$

Representing the square wave excitation of the pneumatic valve, the axial pressure gradient $\partial p/\partial x(t) = (\mathrm{sgn}(\sin(2\pi ft)) + 1)/2$. The compressibility appears as a frequency-dependent density in the inertia term, which becomes increasingly dominant as the frequency approaches f_H.

The numerical solution of Eq. (3) is shown in Fig. 2 for the range of frequencies used in this investigation. Figure 2(a) shows the spatial mean velocity as a function of time within a pulsation period, once periodic equilibrium has been reached. Figure 2(b) shows the cross-stream profiles at two time instances: the dotted and solid lines represent the profiles at the start and end of the ejection phase, respectively. Although the Stokes number is moderately high for these tests ($St = 156$–953), the profile is still relatively parabolic in shape.

At higher frequency (40-55 Hz), the nozzle velocity does not reach zero prior to each ejection phase. Only for the lowest frequency (9 Hz) does the mean velocity resemble a square wave form. This effect is due to the fluid inertia and compressibility, which is inevitable for a gas jet issuing from a finite length pipe nozzle [15]. The effective pulsation amplitude therefore decreases with increasing frequency. As a measure of the effective pulsation amplitude, the rms velocity fluctuation u'_m in Fig. 2(a) equals 100%, 79%, 42% and 19% of the time-averaged mean velocity $\bar{U}_m$ for frequencies 9, 27, 40 and 55 Hz respectively.

4. Experimental Results

4.1. Heat Transfer Results for Steady Flow

Shadlesky [6] used laminar flow theory to derive a lower bound for the stagnation heat transfer rate in an impinging steady jet with a uniform nozzle velocity profile, $Nu_0 = 0.5856 Re^{0.5} Pr^{0.4}$. This theoretical relationship represented by the thin solid line in Fig. 3 is valid for $H/D < 2$. The constant depends on the radial velocity gradient at the stagnation point, $Nu_0/(Re^{0.5} Pr^{0.4}) \propto \beta_0^{1/2}$. Therefore, this is a lower bound for the stagnation heat transfer rate to a pipe jet because of the steeper gradient of a developed velocity profile.

Several studies have investigated the heat transfer to a steady impinging jet issuing from a long pipe nozzle [24–26] yet the heat transfer rates are very sensitive to differences in flow conditions [27–29]. Lytle and Webb [24] used a smooth pipe of 78*D* long to study the heat transfer to an impinging air jet at small nozzle-to-surface spacing ($0.1 \leq H/D \leq 1$). Their correlation for the stagnation Nusselt number is given by the dashed line in Fig. 3 ($Nu_0 = 0.726 Re^{0.53} (H/D)^{-0.191}$ for $3600 \leq Re \leq 27600$). Lee and Lee [25] studied a range of Reynolds numbers from 5000 to 30,000 and H/D = 2–10 using an air jet from a 78*D* long smooth pipe, resulting in a correlation $Nu_0 = 0.443 Re^{0.565} (H/D)^{0.0384}$ (dash-dotted line in Fig. 3). Katti and Prabhu [26] studied a range of Reynolds numbers from 12,000 to 28,000 and H/D = 0.5–8 using an air jet from a 83*D* long smooth pipe. Their stagnation heat transfer data for H/D = 0.5 match those of Lytle and Webb [24]. They adopted a correlation $Nu_0 \propto Re^{0.5} Pr^{1/3} (H/D)^{-0.11}$ by Brdlik and Savin [30], where the proportionality constant varies between 1.15 and 1.63 for H/D = 0.5-8 (dashed line with dot markers in Fig. 3). They compared their results to a theoretical approach by Gauntner et al. [31] for the radial velocity gradient based on the static pressure distribution on the surface. This led to an underprediction of Nu_0 by 25-30% attributed to turbulence near the stagnation point.

The hollow markers in Fig. 3 represent the current experiments for a steady impinging pipe jet at H/D = 1, 2, 3, 4, 6 and Re = 6000 (○), 10,000 (□) and 14,000 (△). The thick solid line represents a least squares fitted power law $Nu_0 = 0.799Re^{0.5}Pr^{0.4}(H/D)^{0.0436}$ (R^2 = 0.42). The Nu_0 values are at the lower end of those obtained in the other pipe flow studies [24–26], which may be attributed to a lower turbulence level or the shorter pipe length (32D compared to 78-83D [24–26]). Figure 4 shows the radial profiles of the local Nusselt number for H/D = 1 (Fig. 4(a)) and H/D = 6 (Fig. 4(b)), which are in good agreement with results by O'Donovan and Murray [21] (dotted line in Fig. 3) using the same pipe nozzle.

4.2. Heat Transfer Results for Pulsating Flow

This section discusses the heat transfer results of an impinging air jet issuing from a circular pipe nozzle (D = 13mm), for Re = 6,000, 10,000, 14,000; H/D = 1, 2, 3, 4, 6; and f = 9, 18, 27, 32, 36, 40, 55 Hz (160 ≤ St ≤ 980; 0.007 ≤ Sr ≤ 0.1). Adopting the definition of the stroke length used for synthetic jets [4] ($L_0/D = \int_{t=0}^{1/(2f)} U_m(t)dt = Sr^{-1}$), 9.6 ≤ L_0/D ≤ 137.

4.2.1 Effect of Pulsation on Local Heat Transfer Profiles

Figure 5 shows the effect of pulsation on the local Nusselt number distribution. The markers represent pulsating flow experiments and the solid lines represent steady flow cases at the same Reynolds number based on the time-averaged mean nozzle velocity. For H/D = 1, the steady flow heat transfer distribution features a secondary peak around r/D = 1.5. This phenomenon is known to occur in impinging jets at low H/D and is attributed to a laminar to turbulent transition in the wall jet [21]. At a low frequency pulsation (f = 9 Hz (○) and f = 27 Hz (□)), Figs. 5(a,b) shows a heat transfer reduction near the stagnation point and an increase near the secondary peak (r/D = 1.5). The peak itself becomes less pronounced although it remains present at the same location. At a higher frequency (f = 40 Hz (△) and f = 55 Hz (◇)), Figs. 5(a,b) shows a heat transfer increase across the entire surface. The secondary peak (still at r/D = 1.5) becomes much more pronounced and its magnitude rivals the stagnation value. Although not shown, a similar behavior is observed for H/D = 2. For H/D = 3-4, a minor secondary peak can still be observed around r/D = 2, which however is not reinforced at higher pulsation frequency. The behavior for H/D ≥ 3 is similar to that shown for H/D = 6 in Figs. 5(c,d).

For H/D = 6, the Nusselt number monotonically decreases from the stagnation point (see Figs. 5(c,d)). When pulsation is applied, the heat transfer distribution shifts upwards across the entire range of r/D, although the relative enhancement compared to steady flow is highest in the wall jet region ($1.5 < r/D < 4$) and lowest in the stagnation zone ($r/D < 1$).

Based on Fig. 5, flow pulsation generally improves the heat transfer rate. The enhancement increases with frequency, although the enhancement does not scale linearly with either frequency (Stokes number $St \propto f$) or Strouhal number $Sr \propto f\, U_m^{-1}$. The two lower frequencies (f = 9 and 27 Hz (○,□)) give similar results, as do the two higher frequencies (f = 40 and 55 Hz (△,◇)). Fig. 5(a) shows the heat transfer distribution at an intermediate frequency (f = 36 Hz (▷)) which features a transition between these two regimes.

Although these two regimes depend on frequency (or Stokes number) and not on Strouhal number, there might be a hidden dependence on the effective pulsation amplitude $u'_m/\overline{U}_m$. As shown in Fig. 2, fluid compressibility inevitably reduces $u'_m/\overline{U}_m$ for increasing frequency. For low frequencies, the mean velocity fluctuates between near zero and a positive flow rate ($u'_m/\overline{U}_m$ = 100% and 79% for 9 and 27 Hz, respectively). For high frequencies, the instantaneous flow does not reach standstill and the pulsating flow resembles a steady flow with a superimposed oscillation ($u'_m/\overline{U}_m$ = 42% and 19% for 40 and 55 Hz, respectively). The existence of these two nozzle flow regimes (see Fig. 2) is demonstrated by the heat transfer profiles in Fig. 5.

Figure 6 shows the radial profiles of the time-averaged Nusselt number Nu and its rms fluctuation $Nu' = \left[(n-1)^{-1} \sum_{i=1}^{n} \left(Nu_i - \overline{Nu} \right)^2 \right]^{1/2}$. This quantity is determined using a surface mounted hot film sensor operated in a constant temperature anemometer bridge, using the approach described in previous studies by the authors [4,8,21]. The time-averaged Nusselt number is obtained using the differential thermopile sensor described in Sect. 2.

For steady flow, the values for $Nu'(r)$ are about 4% of the time-averaged value $Nu(r)$, with a maximum of about 7% at r/D = 1.75 due to the transition to turbulence in the wall jet, corresponding to the secondary peak in the time-averaged Nusselt number profile. For pulsating flow, the Nu' values are significantly higher than for steady flow, about 20-30% of the time-averaged Nusselt number near the stagnation point. A first local maximum of $Nu'(r)/Nu(r)$ = 33-42% can be observed at $r/D \cong 0.6$ and a secondary maximum of 36-48% at $r/D \cong 1.75$.

4.2.2 Effect of Pulsation on Heat Transfer Characteristics

As shown in Fig. 5, flow pulsation increases the heat transfer rate in the wall jet region more than in the stagnation zone. Since the resulting Nusselt distribution widens, the area-averaged Nusselt number $Nu_m = \frac{2}{R^2}\int_{r=0}^{R} Nu(r)\, r\, dr$ (here: R = 6D) is more affected by pulsation than the stagnation point value Nu_0. Figure 7 shows their dependence on the pulsation frequency, with the corresponding steady flow results at the same Reynolds number indicated at f = 0. To isolate the effect of pulsation frequency from the Reynolds number and nozzle-to-surface spacing, the heat transfer data are plotted in Fig. 7(a-c) as a modified Frössling number $Fr = Nu/(Re^{0.5}Pr^{0.4}(H/D)^{0.0436})$, where the exponents are taken from the steady jet characterization (Sect. 4.1, Fig. 3). The solid lines represent the area average Fr_m and the dotted lines represent the stagnation value Fr_0. Figure 7(d-f) shows the same data plotted as heat transfer enhancement δNu relative to steady flow at the same Reynolds number and H/D.

The results in Fig. 7 scale reasonably well with frequency f (Stokes number). For 6000 ≤ Re ≤ 14,000, there is no clear dependence on the Strouhal number ($\propto f\, U_m^{-1}$) as previously suggested by Zumbrunnen and Aziz [13]. The stagnation point heat transfer rate (dotted lines in Fig. 7) decreases to -13% of the steady flow value for H/D = 1 and low frequency pulsation (f = 18 Hz, Re = 10,000, Sr = 0.02) (see Fig. 7(d)). For H/D = 1-2, higher frequencies show a stagnation point enhancement of 4-12% for (f = 55 Hz, Re = 6000-10,000, Sr = 0.06-0.1) (see Fig. 7(d,e)). The highest stagnation point enhancement is 49% at H/D = 6 (f = 55 Hz, Re = 6000, Sr = 0.10) (see Fig. 7(f)).

More consistent and higher enhancements are observed in the area-averaged heat transfer rate (solid lines in Fig. 7) showing a monotonic increase with frequency. Two regimes occur at low and high frequency with a gradual transition around $f \cong$ 35 Hz, as mentioned in the discussion of Fig. 5. The highest area-averaged enhancement is 85% for H/D = 6 (f = 55 Hz, Re = 6000, Sr = 0.10) and 72-75% for H/D = 1-2. The enhancement is more pronounced for lower Reynolds numbers, which suggests a Strouhal number dependence. While H/D strongly affects the stagnation point heat transfer rate, this dependence nearly vanishes for the area-averaged heat transfer.

4.2.3 Scaling the Heat Transfer Enhancement Results

As shown in Figs. 5-7, the heat transfer enhancement due to pulsation behaves differently in the stagnation zone and the wall jet region. This section identifies two appropriate dimensionless groups to scale the enhancement in both regions, encompassing the entire investigated range (H/D = 1, 2, 3, 4 and 6; Re = 6000, 10,000 and 14,000; f = 9, 18, 27, 32, 36, 40 and 55 Hz). The area-averaged enhancement over a region A between two radii is defined as

$$\delta Nu_{m(\text{region } A)} = \frac{\int_{r\in A} Nu^{(\text{pulsating})}(r)\, r\, dr}{\int_{r\in A} Nu^{(\text{steady})}(r)\, r\, dr} - 1 \tag{4}$$

where the limit cases are the stagnation point enhancement $\delta Nu_0 = Nu_0^{(\text{pulsating})}/Nu_0^{(\text{steady})} - 1$ and the overall area-averaged enhancement $\delta Nu_m = Nu_m^{(\text{pulsating})}/Nu_m^{(\text{steady})} - 1$.

For a circular impinging jet with nozzle diameter D, three parameters determine the heat transfer characteristics: pulsation frequency f, the time-averaged mean nozzle velocity U_m and the nozzle-to-surface spacing H. The dimensionless group that best collapses the results is assumed to be a product of the dimensionless equivalents of f, U_m and H (i.e., St, Sr, Re and H/D). The dependencies are determined from the experimental data by least squares fitting a general power law to the heat transfer enhancement:

$$\delta Nu \cong F\left(f, U_m, H\right) = b + a\left(\frac{f\ H^p}{U_m^n}\right)^q \tag{5}$$

where the main interest is in determining the exponents p and n, and thus select the appropriate combination of dimensionless parameters St ($\propto f^1 H^0 U_m^0$), Sr ($\propto f^1 H^0 U_m^{-1}$), Re ($\propto f^0 H^0 U_m^1$) and H/D ($\propto f^0 H^1 U_m^0$).

Table 2 shows the coefficients and exponents by fitting Eq. (5) in four spatial regions. For the stagnation point, the exponents p and n are close to unity, indicating that a modified Strouhal number based on the nozzle-to-surface distance ($f\ H/U_m$) would collapse the results. Similar results are obtained when averaging over a finite stagnation region $0 \le r/D \le 0.5$. For the overall area average, the dependence on U is significantly smaller and the dependence on H is almost negligible. Similar results are obtained when averaging over only the wall jet region ($r/D > 1$).

The following dimensionless groups collapse the δNu results for the stagnation point and the overall average. The least squares fitted coefficients are given in Table 3, and these correlations correspond to the solid lines in Fig. 8. Of the four spatial regions in Table 2, the stagnation point and the overall average are chosen because these are the most commonly used characteristics.

$$\begin{cases} \delta Nu_0 \cong F_0\left(f, U_m, H\right) = b_0 + a_0\left(Sr\left(H/D\right)\right)^{q_0} \\ \delta Nu_m \cong F_m\left(f, U_m\right) = a_m\left(Sr\, Re^{0.5}\right)^{q_m} \end{cases} \tag{6}$$

The markers in Fig. 8 represent the experimental results for the entire investigated range (H/D = 1, 2, 3, 4 and 6; Re = 6000, 10,000 and 14,000; f = 9, 18, 27, 32, 36, 40 and 55 Hz) as a function of the above dimensionless groups. Figure 8(a) shows the stagnation point enhancement δNu_0 as a function of $Sr(H/D)$ (= $f\,H/U_m$), fitted by the first correlation in Eq. (6). Figure 8(b) shows the area-averaged enhancement δNu_m as a function of $Sr(Re)^{0.5}$, fitted by the second correlation in Eq. (6).

For an impinging axisymmetric *synthetic jet*, Persoons et al. [4] identified four regimes for the stagnation point Nusselt number, with thresholds based on the ratio of stroke length to nozzle-to-surface spacing $(L_0 - L_0^{(f)})/H$, where $L_0^{(f)}$ represents the formation threshold for the synthetic jet ($L_0^{(f)}/D \cong 1.5$). Since $L_0/D = Sr^{-1}$, the dimensionless group in Fig. 8(a) $Sr(H/D) = [L_0/H]^{-1}$. Comparing the findings of this study and Persoons et al. [4], the same group scales the stagnation point heat transfer rate to a pulsating jet and to a synthetic jet. Although the investigated ranges in both studies are different (for Persoons et al. [4], $0.2 < Sr(H/D) < 3.3$), this is still an interesting result.

5. Conclusion

The effect of flow pulsation on the local convective heat transfer to an axisymmetric impinging air jet has been investigated. Because of the inconsistencies in the literature, this study set out to confirm the heat transfer behavior of pulsating jets for a wide range of parameters to identify the mechanisms involved. The experiments covered three Reynolds numbers (Re = 6000, 10,000 and 14,000), five nozzle-to-surface distances (H/D = 1, 2, 3, 4 and 6) and seven pulsation frequencies (f = 9, 18, 27, 32, 36, 40, and 55 Hz).

A fast acting pneumatic valve has been used to apply pulsation, switching the flow between two identical branches one of which impinges onto the instrumented heated surface. A theoretical analysis of the nozzle flow velocity (Sect. 3) shows that the effective pulsation amplitude depends on the pulsation frequency. This effect is inevitably caused by fluid compressibility and may introduce a contamination in the results. The effective pulsation amplitude depends on the working fluid (here: air) and the dimensions of the nozzle, which complicates interpreting and comparing the results across different studies.

The effect of flow pulsation on the local heat transfer coefficient distribution has been presented and discussed. The most obvious feature is the markedly different behavior for the stagnation region and the wall jet region. In the wall jet region, a monotonic increase in heat transfer enhancement with increasing frequency can be observed up to a maximum enhancement of +85%, with a negligible dependence on nozzle-to-surface spacing. Close to the stagnation point, the heat transfer rate initially decreases (-13%) for low pulsation frequency and low nozzle-to-surface spacing, yet positive enhancements are seen for higher frequencies. For higher nozzle-to-surface spacing ($H/D > 2$), the stagnation point enhancement is positive and increases up to +50% at the highest frequency and lowest Reynolds number investigated.

While Zumbrunnen and Aziz [13] proposed a Strouhal number criterion for stagnation point heat transfer enhancement, this study has identified two modified Strouhal numbers as the appropriate scaling parameters. The stagnation point enhancement scales well with a modified Strouhal number, $Sr(H/D) = f\ H/U_m$, while the area-averaged enhancement scales well with $SrRe^{0.5}$ ($\propto f\ U_m^{-0.5}$). Using these dimensionless groups, the two power laws in Eq. (6) collapse the entire investigated range with $R^2 \cong 0.8$.

Although the effect of flow pulsation on jet impingement heat transfer still warrants further investigation to fully uncover the heat transfer mechanisms, the present study has provided some more insight into the scaling of the enhancement. Furthermore, the results prove that pulsating jets can achieve very significant enhancements compared to a steady jet of the same flow rate. The enhancement is higher in the wall jet region than near the stagnation point, resulting in a wider, more spatially uniform heat transfer coefficient distribution. Finally, as demonstrated in the literature review, minor changes to the flow configuration (e.g., nozzle geometry, submerged or free surface jets, pulsation wave form, etc) significantly affect the level of enhancement, which should be taken into consideration when comparing the findings between different studies.

Acknowledgments

Dr. Tim Persoons is a Marie Curie research fellow of the Irish Research Council (IRC). Karl Brown is a postgraduate research scholar of the IRC.

References

[1] Garimella S. V., Yeh L.-T., and Persoons T., 2012, “Thermal Management Challenges in Telecommunication Systems and Data Centers,” IEEE Transactions on Components, Packaging and Manufacturing Technology, **2**(8), pp. 1307–1316.

[2] Agostini B., Fabbri M., Park J. E., Wojtan L., Thome J. R., and Michel B., 2007, “State of the art of high heat flux cooling technologies,” Heat Transfer Engineering, **28**(4), pp. 258–281.

[3] Escher W., Michel B., and Poulikakos D., 2010, “A novel high performance, ultra thin heat sink for electronics,” International Journal of Heat and Fluid Flow, **31**(4), pp. 586–598.

[4] Persoons T., McGuinn A., and Murray D. B., 2011, “A general correlation for the stagnation point Nusselt number of an axisymmetric impinging synthetic jet,” International Journal of Heat and Mass Transfer, **54**(17-18), pp. 3900–3908.

[5] Persoons T., O’Donovan T. S., and Murray D. B., 2009, “Heat Transfer in Adjacent Interacting Impinging Synthetic Jets,” Proc. ASME Heat Transfer Summer Conf., San Francisco, CA, Vol. 1: Heat Transfer in Electronic Equipment, ASME, San Francisco, CA, pp. 955–962.

[6] Shadlesky P. S., 1983, “Jet Impingement to a Plane Surface,” AIAA Journal, **21**(8), pp. 1214–1215.

[7] Liu T. S., and Sullivan J. P., 1996, “Heat transfer and flow structures in an excited circular impinging jet,” International Journal of Heat and Mass Transfer, **39**(17), pp. 3695–3706.

[8] O’Donovan T. S., and Murray D. B., 2007, “Effect of acoustic excitation on the heat transfer to an impinging air jet,” Proceedings of the ASME-JSME Thermal Engineering Summer Heat Transfer Conference, Vancouver, BC, Canada, pp. HT2007–32800.

[9] Sheriff H. S. S., and Zumbrunnen D. A. A., 1994, “Effect of flow pulsations on the cooling effectiveness of an impinging jet,” Journal of Heat Transfer, Transactions of the ASME, **116**(4), pp. 886–895.

[10] Azevedo L. F. A., Webb B. W., and Queiroz M., 1994, “Pulsed air jet impingement heat transfer,” Experimental Thermal and Fluid Science, **8**(3), pp. 206–213.

[11] Hofmann H. M., Movileanu D. L., Kind M., and Martin H., 2007, “Influence of a pulsation on heat transfer and flow structure in submerged impinging jets,” International Journal of Heat and Mass Transfer, **50**(17-18), pp. 3638–3648.

[12] Camci C., and Herr F., 2002, “Forced Convection Heat Transfer Enhancement Using a Self-Oscillating Impinging Planar Jet,” Journal of Heat Transfer, **124**(4), p. 770.

[13] Zumbrunnen D. A., and Aziz M., 1993, “Convective heat-transfer enhancement due to intermittency in an impinging jet,” Journal of Heat Transfer, Transactions of the ASME, **115**(1), pp. 91–98.

[14] Herwig H., and Middelberg G., 2008, “The physics of unsteady jet impingement and its heat transfer performance,” Acta Mechanica, **201**(1-4), pp. 171–184.

[15] Mladin E. C., and Zumbrunnen D. A., 1997, “Local convective heat transfer to submerged pulsating jets,” International Journal of Heat and Mass Transfer, **40**(14), pp. 3305–3321.

[16] Behera R. C., Dutta P., and Srinivasan K., 2007, “Numerical Study of Interrupted Impinging Jets for Cooling of Electronics,” **30**(2), pp. 275–284.

[17] Farrington R. B., and Clauncht S. D., 1994, “Infrared Imaging of Large-Amplitude , Low-Frequency Disturbances on a Planar Jet,” AIAA Journal, **32**(2), pp. 317–323.

[18] Smith B. L., and Glezer A., 2001, “The formation and evolution of synthetic jets,” Physics of Fluids, **10**(9), pp. 2281–2297.

[19] Valiorgue P., Persoons T., McGuinn A., and Murray D. B., 2009, “Heat transfer mechanisms in an impinging synthetic jet for a small jet-to-surface spacing,” Experimental Thermal and Fluid Science, **33**(4), pp. 597–603.

[20] Persoons T., Saenen T., Van Oevelen T., and Baelmans M., 2012, “Effect of Flow Pulsation on the Heat Transfer Performance of a Minichannel Heat Sink,” Journal of Heat Transfer, **134**(9), p. 091702.

[21] O'Donovan T. S., and Murray D. B., 2007, "Jet impingement heat transfer – Part I: Mean and root-mean-square heat transfer and velocity distributions," International Journal of Heat and Mass Transfer, **50**(17-18), pp. 3291–3301.

[22] White F. M., 1991, Viscous Fluid Flow, McGraw-Hill, New York.

[23] Beranek L. L., 1996, Acoustics, Acoustical Society of America, Woodbury, NY.

[24] Lytle D., and Webb B. W., 1994, "Air-jet impingement heat-transfer at low nozzle plate spacings," International Journal of Heat and Mass Transfer, **37**(12), pp. 1687–1697.

[25] Lee J., and Lee S. S., 1999, "Stagnation region heat transfer of a turbulent axisymmetric jet impingement," Experimental Heat Transfer, **12**(2), pp. 137–156.

[26] Katti V., and Prabhu S. V., 2008, "Experimental study and theoretical analysis of local heat transfer distribution between smooth flat surface and impinging air jet from a circular straight pipe nozzle," International Journal of Heat and Mass Transfer, **51**(17-18), pp. 4480–4495.

[27] Viskanta R., 1993, "Heat transfer to impinging isothermal gas and flame jets," Experimental Thermal and Fluid Science, **6**(2), pp. 111–134.

[28] Jambunathan K., Lai E., Moss M. A., and Button B. L., 1992, "A review of heat-transfer data for single circular jet impingement," International Journal of Heat and Fluid Flow, **13**(2), pp. 106–115.

[29] Hoogendoorn C. J., 1977, "Effect of Turbulence on Heat-Transfer at a Stagnation Point," International Journal of Heat and Mass Transfer, **20**(12), pp. 1333–1338.

[30] Brdlik P. M., and Savin V. K., 1966, "Heat transfer in the vicinity of the stagnation point in an axisymmetric jet flowing over flat surfaces normal to the flow," Journal of Engineering Physics, **10**(4), pp. 241–245.

[31] Gauntner J. W., Livingood J. N. B., Hrycak P., D- N. A. S. A. T. N., Guzlntner J. W., and Hrycuk P., 1970, "Survey of literature on flow characteristics of a single turbulent jet impinging on a flat plate," NASA Technical Note TN D-5652, NASA, Washington, DC.

List of Table Captions

Table 1. Overview of parameter ranges of selected studies of pulsating jet heat transfer

Table 2. Coefficients of Eq. (5), least-squares fitted to the heat transfer enhancement δNu in four spatial regions. Exponents n and p quantify the dependence of δNu on the jet velocity U_m and the nozzle-to-surface spacing H, respectively.

Table 3. Coefficients of Eq. (6), least-squares fitted to the heat transfer enhancement δNu as a function of two dimensionless groups, $Sr(H/D)$ for the stagnation point and $SrRe^{0.5}$ for the area-average.

List of Figure Captions

Figure 1. Schematic of the impinging pulsating jet test facility. (a) pipe nozzle, (b) dummy pipe nozzle, (c) pneumatic valve, (d) square wave generator and amplifier, (e) mass flow controller, (f) pressure regulator and buffer vessel (not shown), (g) isothermally heated instrumented surface on traversing stage, (h) flush-mounted heat flux and embedded surface temperature sensors, (i) computer with data acquisition system.

Figure 2. Theoretical nozzle velocity for (○) f = 9 Hz (St = 156), (□) 27 Hz (St = 468), (△) 40 Hz (St = 693), (◇) 55 Hz (St = 953). (a) Time-resolved mean velocity $U_m(t)$ and (b) velocity profiles at the start of the ejection phase $U(r, f{\cdot}t = 0)$ (···) and the end $U(r, f{\cdot}t = ½)$ (—).

Figure 3. Heat transfer coefficient at the stagnation point of a steady impinging jet plotted as $Nu_0/(Re^{0.5}Pr^{0.4})$ as a function of nozzle-to-surface spacing H/D.

Figure 4. Local Nusselt number profiles for a steady impinging jet at (a) H/D = 1, (b) H/D = 6.

Figure 5. Local Nusselt number profiles for (a) H/D = 1 and Re = 6000, (b) H/D = 1 and Re = 10,000, (c) H/D = 6 and Re = 6000 and (d) H/D = 6 and Re = 10,000. The solid line represents steady flow. Markers represent pulsating flow at f = 9 Hz (○), 27 Hz (△), 36 Hz (◇), 40 Hz (▷), 55 Hz (□).

Figure 6. Local time-averaged (—) and fluctuating (– –) Nusselt number profiles for H/D = 2 and (a) Re = 6000 and (b) Re = 10,000. The solid and dashed lines represent steady flow. Markers represent pulsating flow at f = 9 Hz (○) and 55 Hz (□).

Figure 7. Frequency dependence of the area-averaged (—) and stagnation point heat transfer rate (···) plotted as (a-c) Frössling number $Fr = Nu/(Re^{0.5}Pr^{0.4}(H/D)^{0.0436})$ and (d-f) heat transfer enhancement δNu, for H/D = 1 (a), 2 (b) and 6 (c), and Re = 6000 (○), 10,000 (□) and 14,000 (△).

Figure 8. Scaling of (a) stagnation point and (b) area-averaged heat transfer enhancement δNu as a function of $Sr(H/D)$ and $Sr(Re)^{0.5}$. Markers represent the experimental data, with solid and hollow markers for H/D = 1-2 and 3-6, respectively.

List of Tables

Table 1. Overview of parameter ranges of selected studies of pulsating jet heat transfer

Source	**Configuration**	**Reynolds number *Re***	**Pulsation frequency *f* (Strouhal number *Sr*)**	**Nozzle-to-surface spacing**	**Heat transfer enhancement δNu (%)**
1996 Liu and Sullivan [7]	Acoustically excited air jet from contoured nozzle[C,S,U]	12,300	$950\text{Hz} \le f \le 1750\text{Hz}$ ($0.5 \le Sr \le 3.5$)	$0.6 \le H/D \le 2$	$\delta Nu_0 \cong 0$ and $-10\% \le \delta Nu(r) \le +10\%$ ($1 \le r/D \le 2$)
2008 O'Donovan and Murray [8]	Acoustically excited air jet from contoured nozzle[C,S,U]	10,000 - 30,000	$315\text{Hz} \le f \le 630\text{Hz}$ ($0.02 \le Sr \le 0.11$)	$0.5 \le H/D \le 2$	$\delta Nu_0 \cong 0$ and $-21\% \le \delta Nu(r) \le -3\%$ ($1 \le r/D \le 2$)
1994 Sheriff and Zumbrunnen [9]	Pulsating free-surface water jet [C,FS]	2500 - 10,000	$5\text{Hz} \le f \le 280\text{Hz}$ ($0.014 \le Sr \le 0.96$)	$2 \le H/D \le 6$	$-60\% \le \delta Nu_0 \le -18\%$ and $\delta Nu(r \ge D) \cong 0$
2007 Hofmann et al. [11]	Pulsating air jet from contoured nozzle[C,S,U]	14,000 - 78,000	$2\text{Hz} \le f \le 400\text{Hz}$ ($0.001 \le Sr \le 0.2$)	$2 \le H/D \le 8.5$	For $Sr << 0.2$, $H/D > 2$, $\delta Nu_0 = -50\%$ For $Sr = 0.2$, $H/D = 2$, $\delta Nu_0 = +40\%$
2002 Camci and Herr [12]	Self-oscillating planar air jet[P,S]	7500 - 14,000	$20\text{Hz} \le f \le 100\text{Hz}$ ($0.007 \le Sr \le 0.033$)	$24 \le H/D \le 60$	For $H/D = 24$, $+55\% \le \delta Nu_0 \le +70\%$
1993 Zumbrunnen and Aziz [13]	Intermittent planar free-surface water jet[P,S]	3100 - 20,750	$31\text{Hz} \le f \le 142\text{Hz}$ ($0.06 \le Sr \le 0.37$)	$H/D \cong 10$	For $Sr = 0.25$, $\delta Nu_0 = +100\%$ For $Sr < 0.1$, $-20\% < \delta Nu_0 < 0$
2008 Herwig and Middelberg [14]	Pulsating air jet from pipe nozzle[C,S,D]	7500	$1.25\text{Hz} \le f \le 40\text{Hz}$ ($0.003 \le Sr \le 0.08$)	$H/D = 6$	For $Sr = 0.08$, $\delta Nu_0 = +25\%$ For $Sr < 0.01$, $-10\% < \delta Nu_0 < 0$
1997 Mladin and Zumbrunnen [15]	Pulsating planar air jet[P,S,U]	1000 - 11,000	$20\text{Hz} \le f \le 80\text{Hz}$ ($0.003 \le Sr \le 0.106$)	$H/D \cong 10$	For $Sr = 0.106$, $\delta Nu_0 = +12\%$ and $\delta Nu(r \ge D) \le +80\%$
2007 Behera et al. [16]	Pulsating air jet[C,S,U]	5130 - 8560	$25\text{Hz} \le f \le 400\text{Hz}$ ($0.008 \le Sr \le 0.13$)	$5 \le H/D \le 9$	For $Sr = 0.13$, $H/D = 7$, $\delta Nu_0 = +12\%$ and $\delta Nu(r \ge D) \le +35\%$
Present study	Pulsating air jet from pipe nozzle[C,S,D]	6000 - 14,000	$9\text{Hz} \le f \le 55\text{Hz}$ ($0.007 \le Sr \le 0.10$)	$1 \le H/D \le 2$	$\delta Nu_m = +75\%$ ($SrRe^{0.5} \cong 8$, $Sr = 0.1$), $-13\% < \delta Nu_0 < 12\%$ ($0.02 < Sr(H/D) < 0.1$)
				$3 \le H/D \le 6$	$\delta Nu_m = +85\%$ ($SrRe^{0.5} \cong 8$, $Sr = 0.1$) $+20\% < \delta Nu_0 < +50\%$ ($0.2 < Sr(H/D) < 0.6$)

Notes: C = circular nozzle / P = planar nozzle, S = submerged jet / FS = free surface jet, U = uniform velocity profile (contoured nozzle) / D = developed velocity profile (long pipe nozzle)

Table 2. Coefficients of Eq. (5), least-squares fitted to the heat transfer enhancement δNu in four spatial regions. Exponents n and p quantify the dependence of δNu on the jet velocity U_m and the nozzle-to-surface spacing H, respectively.

Region	Dependent variable	Independent variable	Coefficients b	a	q	p	n	R^2
Stagnation point ($r = 0$)	δNu_0	$f\,H^p/U_m^n$	-0.071	0.27	1.06	**0.78**	**0.71**	0.81
Stagnation zone average ($r/D < 0.5$)	$\delta Nu_{m\,(r/D<0.5)}$		-0.063	0.23	1.11	**0.66**	**0.79**	0.82
Wall jet average ($r/D > 1$)	$\delta Nu_{m\,(r/D>1)}$		0 (*)	0.094	0.846	**0.12**	**0.56**	0.83
Overall area average	δNu_m		0 (*)	0.087	0.861	**0.13**	**0.54**	0.83

(*) Not included in least squares fit, and forced to zero.

Table 3. Coefficients of Eq. (6), least-squares fitted to the heat transfer enhancement δNu as a function of two dimensionless groups, $Sr(H/D)$ for the stagnation point and $SrRe^{0.5}$ for the area-average.

Zone	Dependent variable	Independent variable	Coefficients					R^2
			b	***a***	***q***	*p*	*n*	
Stagnation point	δNu_0	$Sr(H/D)$	**-0.079**	**0.805**	**0.836**	1	1	0.80
Overall area average	δNu_m	$SrRe^{0.5}$	—	**0.121**	**0.884**	0	0.5	0.81

List of Figures

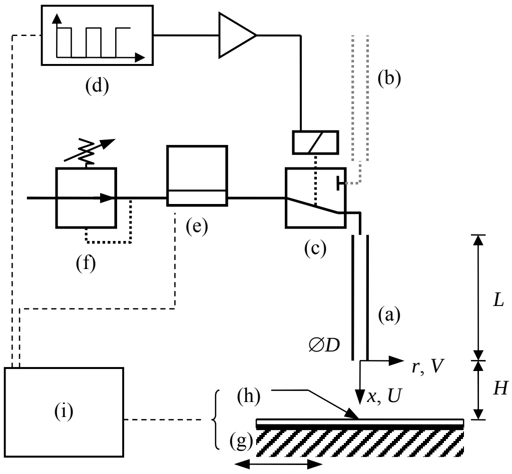

Figure 1

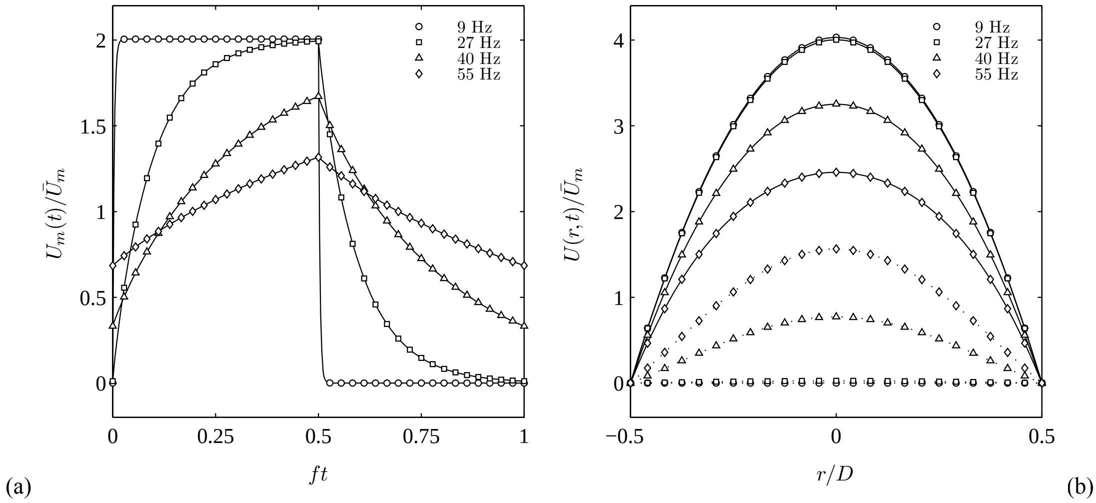

Figure 2

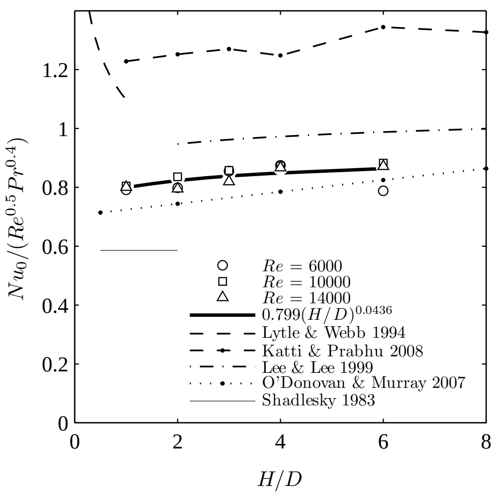

1.2
1
0.8
0.6
0.4
0.2
0
0
2
4
6
8
$Nu_0/(Re^{0.5}Pr^{0.4})$
H/D
$Re = 6000$
$Re = 10000$
$Re = 14000$
$0.799(H/D)^{0.0436}$
Lytle & Webb 1994
Katti & Prabhu 2008
Lee & Lee 1999
O'Donovan & Murray 2007
Shadlesky 1983

Figure 3

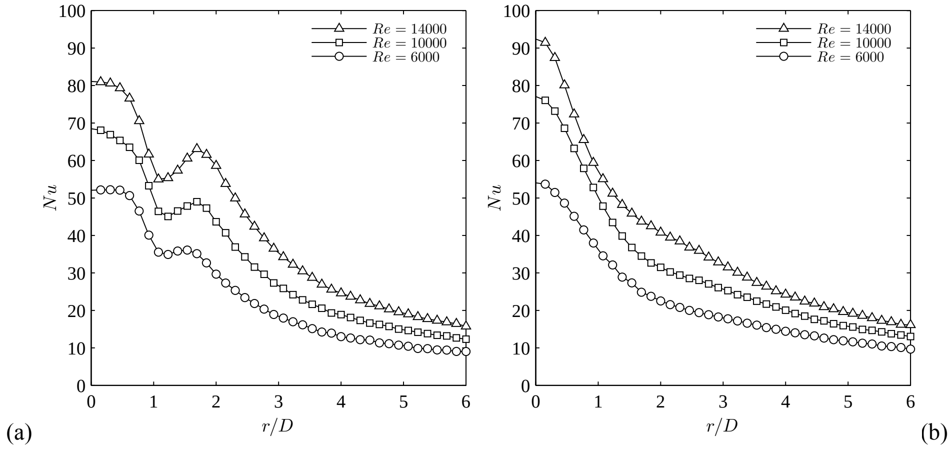

Figure 4

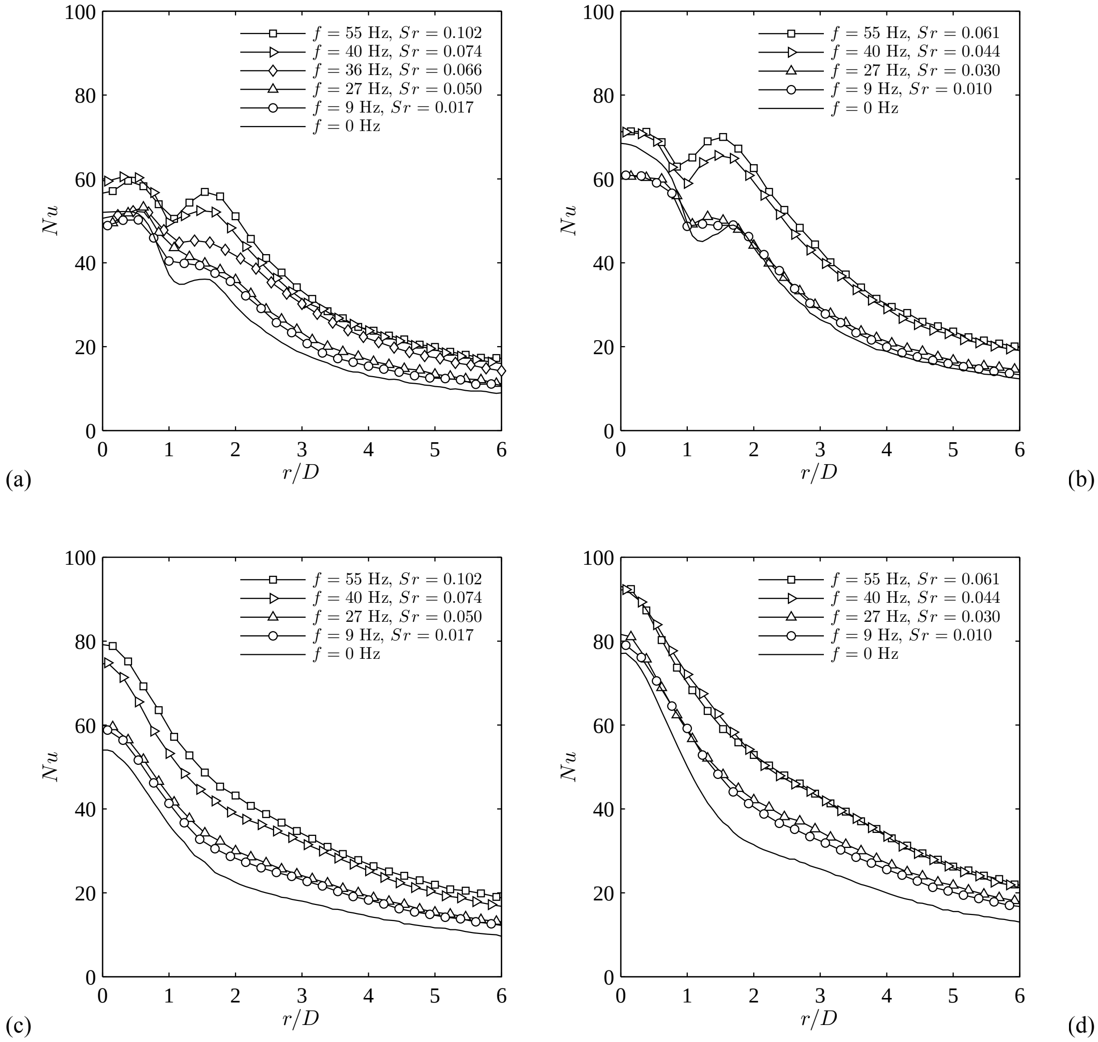
(a)
$f = 55$ Hz, $Sr = 0.102$
$f = 40$ Hz, $Sr = 0.074$
$f = 36$ Hz, $Sr = 0.066$
$f = 27$ Hz, $Sr = 0.050$
$f = 9$ Hz, $Sr = 0.017$
$f = 0$ Hz
(b)
$f = 55$ Hz, $Sr = 0.061$
$f = 40$ Hz, $Sr = 0.044$
$f = 27$ Hz, $Sr = 0.030$
$f = 9$ Hz, $Sr = 0.010$
$f = 0$ Hz
(c)
$f = 55$ Hz, $Sr = 0.102$
$f = 40$ Hz, $Sr = 0.074$
$f = 27$ Hz, $Sr = 0.050$
$f = 9$ Hz, $Sr = 0.017$
$f = 0$ Hz
(d)
$f = 55$ Hz, $Sr = 0.061$
$f = 40$ Hz, $Sr = 0.044$
$f = 27$ Hz, $Sr = 0.030$
$f = 9$ Hz, $Sr = 0.010$
$f = 0$ Hz
Nu
r/D
0
20
40
60
80
100
0
1
2
3
4
5
6

Figure 5

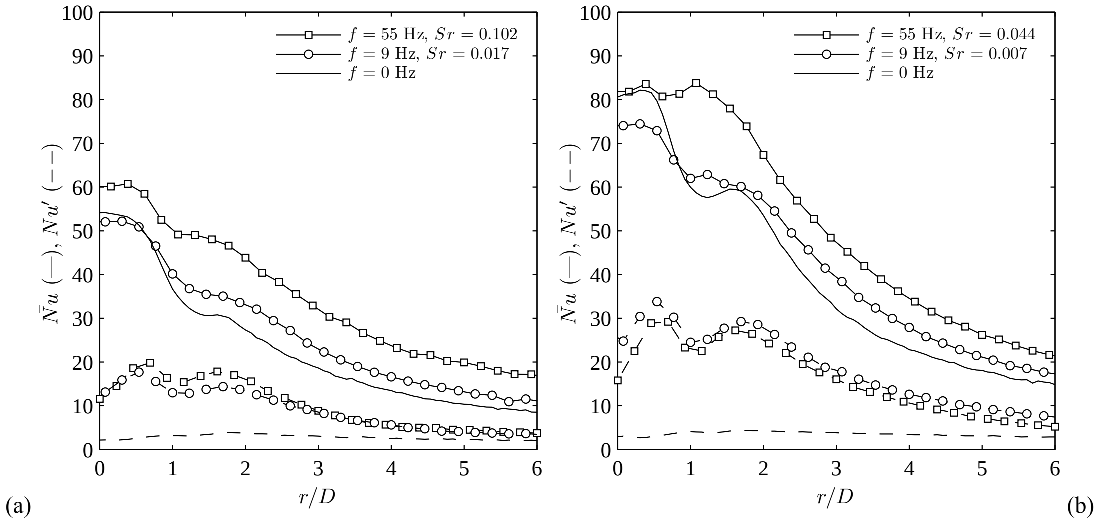
$f = 55$ Hz, $Sr = 0.102$
$f = 9$ Hz, $Sr = 0.017$
$f = 0$ Hz
$\bar{Nu}$ (—), Nu' (− −)
r/D
(a)
$f = 55$ Hz, $Sr = 0.044$
$f = 9$ Hz, $Sr = 0.007$
$f = 0$ Hz
$\bar{Nu}$ (—), Nu' (− −)
r/D
(b)

Figure 6

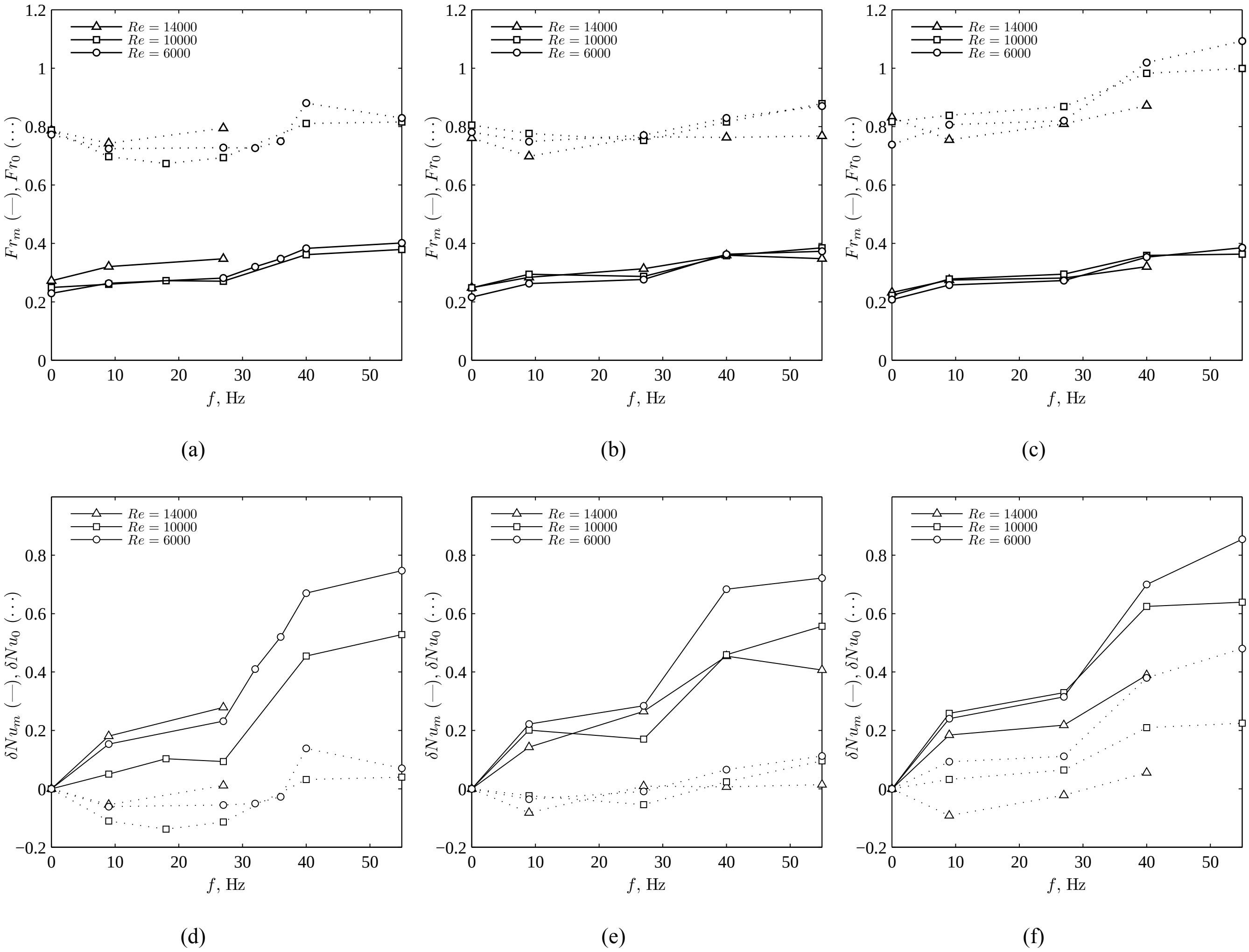
$Re = 14000$
$Re = 10000$
$Re = 6000$
Fr_m (—), Fr_0 (···)
δNu_m (—), δNu_0 (···)
f, Hz
(a)
(b)
(c)
(d)
(e)
(f)

Figure 7

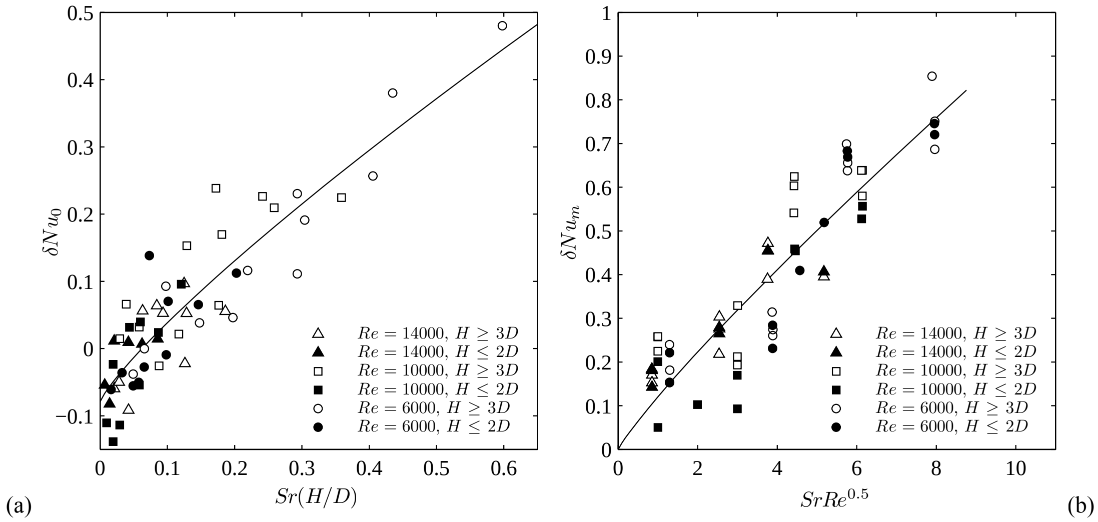

(a)
(b)
δNu_0
$Sr(H/D)$
δNu_m
$SrRe^{0.5}$
$Re = 14000,\ H \geq 3D$
$Re = 14000,\ H \leq 2D$
$Re = 10000,\ H \geq 3D$
$Re = 10000,\ H \leq 2D$
$Re = 6000,\ H \geq 3D$
$Re = 6000,\ H \leq 2D$

Figure 8